Picometer Accuracy in Measuring Lattice Displacements Across Planar Faults by Interferometry in Coherent Electron Diffraction

Lijun Wu, Yimei Zhu,* and J. Tafto†

Materials Science Division, Brookhaven National Laboratory, Upton, New York 11973

(Received 12 June 2000)

We calculate the shadow image in far field below a thin crystal when a coherent electron source is placed at micrometer distances above the specimen, and note that the presence of a planar fault results in very strong oscillatory contrast. We realize these predictions experimentally using a field-emission electron source in a microscope. With this technique, we determine displacement vectors at planar faults with an accuracy down to 1 pm in studies of the $Bi_2Sr_2CaCu_2O_8$ superconductor containing thin intercalated layers.

PACS numbers: 61.72.Nn, 61.16.Bg, 74.72.Hs

In his earliest papers on holography, Gabor [1] suggested placing a coherent electron probe in front of a thin specimen and observing the intensity variations in the shadow image. This technique is referred to as in-line holography. However, rather than in-line holography, off-line or off-axis holography, based on splitting a coherent beam, became the more successful technique both in visual light holography using a laser [2], and in electron holography using a coherent electron source [3]. With the advent of small coherent electron sources based on field-emission guns, in-line electron holography has become feasible [4]. In-line electron holography and the closely related coherent electron diffraction [5] have mostly been used to study the fringes that appear when convergent beam diffraction disks from a perfect crystal overlap. Such experiments provide information about the spatial coherence of the electron source and, in principle, also about the phase of structure factors [6–8].

We present the *first* study where an experimental setup similar to that originally proposed by Gabor to record an electron hologram results in more accurate measurements than available electron microscopic techniques. We form a small coherent electron probe close to the specimen, and show that accurate measurements of lattice displacements can be obtained in this way. We realize this experimentally with a 300 kV state-of-the-art transmission electron microscope equipped with a field-emission gun, using the prespecimen lenses of the microscope to form a small electron probe at a crossover adjustable to the desired height above the specimen. We study the high-temperature superconductors $Bi_2Sr_2CaCu_2O_8$ (Bi-2212), and determine the translation vector between two crystal grains separated by a planar fault with an accuracy better than previously achieved with established techniques.

In Gabor's in-line holography, a great part of the diverging electrons illuminates areas outside the specimen and acts as a reference to record the phase information that characterizes a hologram. Our purpose is to study defects, which are deviations from perfect crystal structure, so we let all electrons propagate through the specimen, and the electrons that propagate on one side of the defect may be looked upon as the reference wave field. In this study we use a small divergence of the incident beam and restrict our study to the measurement of displacement vectors associated with planar faults. Thus, in the following, we use the term coherent electron diffraction rather than holography.

To calculate the convergent beam electron diffraction pattern that forms in far field when a coherent point source is placed at micrometer distances above the specimen, we consider the phase difference for different paths from the source through the specimen for electrons scattered in a certain direction. We start with the one-dimensional case indicated in Fig. 1. Here, the short vertical lines represent atomic planes separated by a distance c. H is the distance from the probe, or crossover, to the specimen, R is the horizontal displacement at the fault that is placed at the

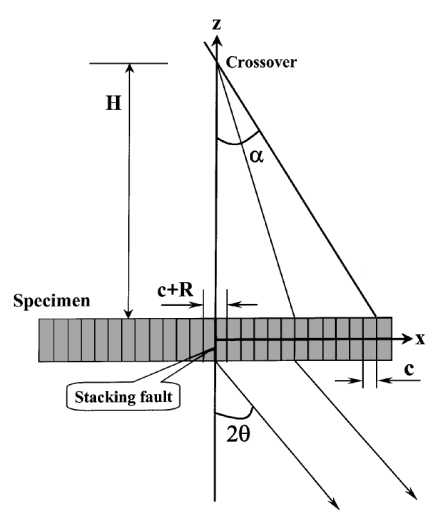

FIG. 1. Schematic of the experimental setup. The short vertical lines represent in the simplest situation of atom planes with spacing c. H is the distance from the source, of crossover, to the specimen, R is the horizontal displacement at the fault that is placed at the vertical mirror in the figure, and α is the convergent beam angle also defining the illuminated area on the specimen.

 0031-9007/00/85(24)/5126(4)$15.00 © 2000 The American Physical Society

vertical mirror in the figure, 2θ is the angle relative to the vertical axis, λ_0 is the electron wavelength, and $F(\theta)$ is the scattering amplitude of the slice of the crystal represented by one of the vertical lines in Fig. 1:

$$\varphi(\theta) = \sum_{n=1}^{2N} F(\theta) \exp\left(2\pi i \frac{\sqrt{x_n^2 + H^2} - x_n \sin 2\theta}{\lambda_0}\right). \tag{1}$$

Here the distance x_n is

$$x_n = \begin{cases} (n - N)c - (c/2 + R/2) & n \leq N, \\ (n - N - 1)c + (c/2 + R/2) & n > N. \end{cases}$$

The summation is over the whole illuminated area; that is $|x_n| \leq r_{\max}$ where $r_{\max}$ is the radius of the beam at the specimen with $N = (2r_{\max} + c - R)/2c$. The convergent beam angle is $2\alpha = 2r_{\max}/H$ and the intensity $I = \varphi\varphi^*$. In two dimensions, Eq. (1) becomes

$$\varphi_g = \sum_{m,n} F_g \exp 2\pi i \left(\frac{\sqrt{r^2 + H^2}}{\lambda_0} - \vec{r} \cdot \vec{g}\right), \tag{2}$$

where $\vec{g}$ is the reciprocal vector. The position vector of the lattices is given by

$$\vec{r} = \begin{cases} m\vec{a} + (n - N)\vec{c} - (\vec{c}/2 + \vec{R}/2) & n \leq N, \\ m\vec{a} + (n - N - 1)\vec{c} + (\vec{c}/2 + \vec{R}/2) & n > N, \end{cases}$$

where $\vec{a}$ and $\vec{c}$ are basis vectors in the projection.

Figure 2 shows the calculated diffraction disks based on Eq. (2) for different R and H. In Fig. 2(a) with $R = 0$, there is no contrast within the disks, except for the Fresnel diffraction of the circular aperture, as expected for a perfect crystal with no overlap between the diffraction disks. When we introduce a displacement vector $R = c/4$ perpendicular to the incident beam direction, we see interference fringes in reflections where $\vec{g} \cdot \vec{R}$ differs from an integer; while when $\vec{g} \cdot \vec{R}$ is equal to an integer, there is no contrast, as is the case for the 004 reflection. This agrees with what we know from conventional diffraction studies [9,10]. A difference from conventional imaging, however, is that, with the coherent probe close to the specimen, strong contrast is seen simultaneously in many reflections, including high-order ones, when the electrons propagate nearly parallel to the interface, i.e., the interface is viewed edge on. This contrast fades away with increasing distance between the specimen and probe, as seen by comparing Figs. 2(b) and 2(d). With further increase in H, these disks will eventually correspond to conventional dark-field images. The advantage of our approach is that we observe simultaneously a large number of diffraction disks; each of them is a shadow image of the illuminated area. The contrast in the central disk and the reflection disks can be related to the out-of-focus bright-field (BF) and dark-field electron microscopy images. The strongest contrast is seen for $\vec{g} \cdot \vec{R} = 0.5$, and the fringes are asymmetric for odd-index reflections. These features can be used to determine the sign of the displacement. We note that the asymmetric contrast is mirrored around the center of each odd-order reflection when the displacement vector is changed from $R = c/4$ in Fig. 2(b), to $R = -c/4$ in Fig. 2(c).

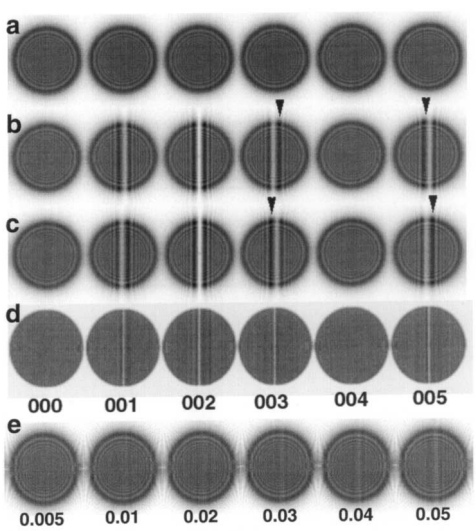

FIG. 2. (a)–(d) The effect of the displacement R and the distance H for reflections of 000–005 of a test crystal. (a) $R = 0$, (b) $R = c/4$, (c) $R = -c/4$, (a)–(c) $H = 160\ \mu$m, and (d) $R = c/4$, $H = 1600\ \mu$m. The arrow pairs in (b) and (c) indicate the reversal of the asymmetry of the fault contrast, which can be used to determine the sign of the displacement. (e) shows the contrast for different phase shifts which can be used to determine the accuracy of the measurements. The phase shifts are indicated in fractions of 2π below the disks.

These calculations are in agreement with the predictions of Cowley [11]. For a perfect crystal of uniform thickness, each nonoverlapping diffraction disk would be the same as that with a noncoherent probe with a one-to-one correspondence between a point on the specimen and a point in each of the disks. However, for a sample that is not perfectly periodic in the directions perpendicular to the beam, the interference effects caused by the coherence of the probe give intensity distributions in the diffraction patterns that depend on the deviation from periodicity.

The structural defects in superconducting oxides have been studied intensively in the last decade because of their influence on flux-pinning and current-carrying capacities [12]. We have used coherent electron diffraction to address planar defects, namely, (001) twist boundaries and stacking faults associated with intercalated layers in $Bi_2Sr_2Ca_{n-1}Cu_nO_{2n+4}$ ($n = 1$, 2, or 3). The lattice parameters a and b are approximately 0.540 nm, but vary slightly with n, while $c = 2.4369$ nm for $n = 1$ [13], $c = 3.087$ nm for $n = 2$ [14], and $c = 3.7074$ nm for $n = 3$ [15]. We limit this brief presentation to two examples of intercalations on the (001) plane of Bi-2212 that illustrate the accuracy of the technique. Measurements of displacements across twist boundaries will be published separately.

In our experiments, diffraction patterns, or shadow images, were in most cases recorded on imaging plates. Energy-filtered shadow images of pertinent diffraction

disks were obtained with the Gatan Imaging Filter and digitally acquired with the attached CCD camera. Figure 3(a) is a real-space image with the crossover above a sample of Bi-2212. It exhibits Fresnel fringes at the rim of the illuminated area, as well as a lattice image of the crystal. The periodicity of the image corresponds to half a unit cell of Bi-2212 along the c axis. A careful inspection of the lattice image suggests a stacking fault in this area, as indicated by arrows. The contrasts from this planar fault are much more visible in the shadow dark-field images, as demonstrated in Figs. 3(b)–3(h) and Fig. 4. In the experimental pattern of Fig. 3(b), the first reflection on the 001 row which is nearly lacking contrast is the $0, 0, 10$, suggesting a displacement vector R close to $c/10 = 0.3087$ nm [Fig. 3(d)]. A displacement of $c/5 = 0.6174$ nm can be ruled out because of the additional extinction at the 115 reflection [Fig. 3(c)].

The intensity in a diffraction disk depends on the value of the structure factor. Furthermore, for increasing crystal thickness, the intensity of one reflection also depends on the structure factors of other reflections through dynamical coupling. In previous studies under similar experimental situations, except for a noncoherent source, we have taken advantage of this dynamical coupling to address charge transfer in superconductors by determining accurately the values of structure factors [16,17]. When the electron probe illuminates a thin flat area of the specimen, the features within the diffraction disks are to a large extent caused by the displacement vector R and the distance H between the crossover and the specimen. Thus, the values of the structure factors serve mainly to scale the intensity of the individual disks. In the following we have omitted this scaling which, in the kinematical case, i.e., a very thin foil with negligible dynamical coupling, is the same as dividing the intensity within each disk by the structure factor squared. Calculation with the displacement vector $c/10 = 3.087$ nm is shown in Fig. 3(d). For larger g vectors the sensitivity to displacement increases. We notice from the experimental pattern in Fig. 4(a) that it is the $1, 1, 29$ rather than the $0, 0, 30$ reflection that is closest to featureless, and this corresponds to a displacement of $3c/29 = 0.319$ nm. By further simulations and comparisons with experiment, focusing particularly on the $1, 1, 29$ disk, we note that a displacement $R = 0.322$ nm, Fig. 4(c), gives too strong a contrast, while the best fit to experiment, Fig. 4(b), was for $R = 0.320$ nm, Fig. 4(d).

Another type of fault we studied also has weak contrast for $l = 10$, 20, and 30, and extinction for $l = 29$. However, by comparing the energy-filtered experimental disks in Figs. 3(e) and 3(g), we note that the asymmetry of the fringe contrast of the fault in Fig. 3(g) is reversed compared with the fault in Fig. 3(e). The reversed positions of the vertical, wide black fringes are evident in the 008 and 0012 reflections, suggesting an opposite sign of the displacement vector. While the contrast from the fault we presented in Fig. 3(e) fits with the contrast asymmetry of the extrinsic fault in Fig. 2(b), the fault in Fig. 3(g) fits with the contrast asymmetry of the intrinsic fault in Fig. 2(c). This is confirmed in the simulation shown in Figs. 3(f) and 3(h).

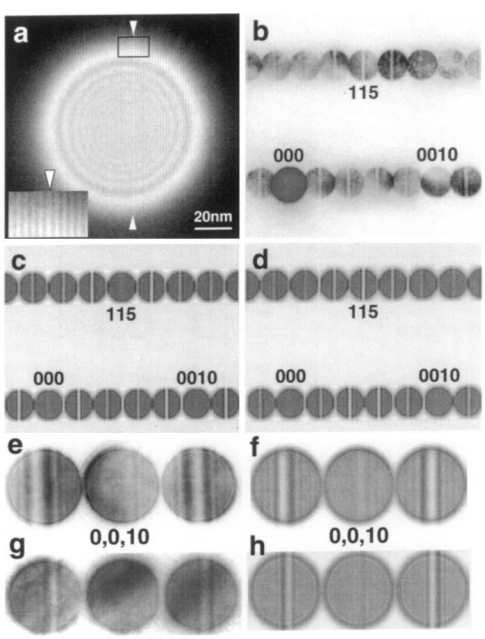

FIG. 3. (a)–(f) show an extrinsic stacking fault due to the addition of a $(Ca + CuO_2)$ layer in $Bi_2Sr_2CaCu_2O_8$. (a) A real-space image (002 lattice fringes) with the crossover above the sample. The inset is an enlargement of the boxed area, showing a wide lattice fringe at the location of the fault denoted by an arrow. (b) Experimental diffraction pattern of the $(1-10)^*$ zone recorded on a film negative. (c),(d) Calculated patterns using the kinematical approach with $R = d_{005} = 0.6174$ nm (c) and $R = d_{0010} = 0.3087$ nm (d). (e) 008–0012 reflections recorded with a zero-loss energy-filtered CCD camera. (f) Calculated diffraction pattern with $R = 0.322$ nm giving a best fit to the 008–0012 reflections in (e). (g),(h) show an intrinsic fault due to the removal of a $(Ca + CuO_2)$ layer in $Bi_2Sr_2CaCu_2O_8$. (g) 008–0012 reflections recorded with a zero-loss energy-filtered CCD camera. (h) Calculated diffraction pattern with $R = 0.319$ nm giving a best fit in (g).

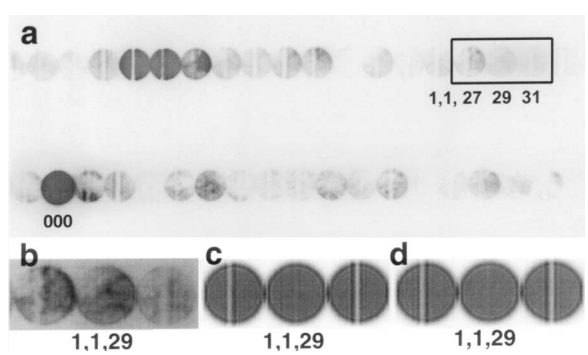

FIG. 4. An extrinsic stacking fault due to the intercalation of a $(Ca + CuO_2)$ layer in $Bi_2Sr_2CaCu_2O_8$. Diffraction pattern near the $(1-10)^*$ zone, recorded with an imaging plate system, showing high-order reflections. (b) Enlarged reflections of $1, 1, 27$, $1, 1, 29$, and $1, 1, 31$. (c),(d) Calculated reflections for $R = 0.322$ nm (c) and $R = 0.320$ nm (d).

We estimate the accuracy in the measurements by using the expression $|\Delta R| = |\Delta n/g|$. Here, Δn is the deviation from the integer n associated with the nth order reflection g. Figure 2(e) shows the residual contrast for $\Delta n = 0.005-0.05$ which can be used as an initial guideline to estimate the accuracy of the measurement. We note that the fault contrast increases with increasing Δn. With this interferometric method at optimum convergent beam angle and height from specimen to crossover, we estimate that the fault exhibits sufficient contrast for $\Delta n \geq 0.01$, similar to the value for BF imaging [18]. However, with the method we use, we observe the contrast in many reflections simultaneously, especially high-order reflections, and thereby improving the information content and accuracy. Based on the simulations we have performed, some of them shown in Figs. 3 and 4, we arrive at $R = 0.320 \pm 0.002$ nm for the extrinsic fault, and $R = -0.319 \pm 0.001$ nm for the intrinsic one. Here, the error ranges were derived from a quantitative $\chi^2 = \Sigma(I^{\mathrm{exp}} - I^{\mathrm{cal}})^2/\Sigma(I^{\mathrm{exp}})^2$ analysis with $\chi^2 < 0.06$. In high-resolution microscopy, an accuracy of one hundredth of nm has been achieved in the determination of displacement across planar faults in diamond [19], and a higher accuracy was reported in a study of antiphase boundaries in GaAs based on conventional BF images [20]. Coherent beam electron diffraction has the potential of an even higher accuracy than the 1 pm reported in this study. This is an interferometric technique, and thus the resolution is not limited by the wavelength of the electrons, but rather by the number of lattice planes on each side of the fault that contribute to the Bragg reflections. In that sense it is similar to a spectrometer where the accuracy of the wavelength determination is inversely proportional to the number of lines in the grating.

The extrinsic and intrinsic stacking faults in Bi-2212, associated with inserting and taking out a slice from the crystal consisting of a (CuO_2 + Ca) layer, result in the replacement of half a unit cell along the c axis of Bi-2212 by half a unit cell of $Bi_2Sr_2Ca_2Cu_3O_{10}$ (Bi-2223) or $Bi_2Sr_2CuO_6$ (Bi-2201), respectively. Based on the reported values of the lattice parameters along the c axis, half a unit cell of Bi-2223 and of Bi-2201 are 0.310 nm longer and 0.325 nm shorter, respectively, than half a unit cell of Bi-2212. Our measurements deviate significantly from these values. This may not come as a surprise considering the strain caused by the constraint that the layers are intercalations in Bi-2212 with a slightly different area of the unit cell in the a-b plane. What we observe is that, within the experimental accuracy of 1–2 pm, the material shrinks or expands $\frac{3}{29}$ of the lattice parameter c by the subtraction or addition of a slab from Bi-2212 consisting of a (CuO_2 + Ca) layer. This fractional displacement corresponds to 0.319 nm for the reported value of $c = 3.087$ nm [14].

In summary, by forming an electron probe close to a specimen in a manner similar to that originally proposed by Gabor to record a hologram, we have measured accurately the displacement associated with planar faults. This interferometric approach is unique in that there are no adjustable microscope parameters, the contrast is strong even when the fault is viewed edge on, a large number of shadow images of the fault corresponding to different Bragg reflections can be studied simultaneously, and the accuracy is, to our knowledge, the highest that has been achieved in measurements of displacement vectors.

This work was supported by the Division of Materials Sciences, U.S. Department of Energy, under Contract No. DE-AC02-98CH10886.

*Corresponding author.
Email address: zhu@bnl.gov
†Visiting scientist from University of Oslo, Norway.

[1] D. Gabor, Nature (London) **161**, 777 (1948).
[2] E.N. Leith and J. Upatnieks, J. Opt. Soc. Am. **52**, 1123 (1962).
[3] G. Mollenstedt and H. Wahl, Naturwissenschaften **55**, 340 (1968).
[4] J.M. Cowley, Ultramicroscopy **41**, 335 (1992); Phys. Rev. Lett. **84**, 3618 (2000).
[5] J.M. Zuo and J.C.H. Spence, Philos. Mag. A **68**, 1055 (1993).
[6] J.C.H. Spence and J.M. Cowley, Optik **50**, 129 (1978).
[7] K. Tsuda, M. Terauchi, M. Tanaka, T. Kaneyama, and T. Honda, in *Proceedings of ICEM-Paris, 1994* (Les Editions de Physique, Paris, 1994), Vol. 1, p. 865.
[8] W.J. Vine, R. Vincent, P. Spellward, and J.W. Steeds, Ultramicroscopy **41**, 42 (1992).
[9] J.M. Cowley and J.C.H. Spence, Ultramicroscopy **6**, 359 (1981).
[10] M. Pan, J.M. Cowley, and J.C. Barry, Ultramicroscopy **30**, 385 (1989).
[11] J.M. Cowley, in *Electron Diffraction Techniques,* edited by J.M. Cowley (Oxford University Press, New York, 1992), Vol. 1, p. 441.
[12] Z. Cai and Y. Zhu, *Microstructures and Structural Defects in High-Temperature Superconductors* (World Scientific, Singapore, 1998); Y. Zhu *et al.,* Philos. Mag. A **70**, 969 (1994); Phys. Rev. B **57**, 8601 (1998) .
[13] C.C. Torardi, M.A. Subramanian, J.C. Calabrese, J. Gopaakeishnan, E.M. McCarron, K.J. Morrissey, T.R. Askew, R.B. Flippen, U. Chowdhry, and A.W. Sleight, Phys. Rev. B **38**, 225 (1988).
[14] Y. Gao, P. Lee, P. Coppens, M.A. Subramanian, and A.W. Sleight, Science **241**, 954 (1988).
[15] G. Miehe, T. Vogt, H. Fuess, and M. Wilhelm, Physica (Amsterdam) **171C**, 339 (1990).
[16] J. Tafto, Y. Zhu, and L. Wu, Acta Crystallogr. Sect. A **54**, 532 (1998).
[17] L. Wu, Y. Zhu, and J. Tafto, Phys. Rev. B **59**, 635 (1999).
[18] P.B. Hirsch, A. Howie, R.B. Nicholson, D.W. Pashley, and M.J. Whelan, *Electron Microscopy of Thin Crystals* (Krieger, Huntington, New York, 1977), 2nd ed., p. 165.
[19] P. Humble, J.K. Mackenzie, and A. Olsen, Philos. Mag. A **52**, 605 (1985).
[20] D.R. Rasmussen, S. McKernan, and C.B. Carter, Phys. Rev. Lett. **66**, 2629 (1991).